



SPE 102151

Robust and Efficient Simulation of Formation-Tester Measurements with a Rigorous Compositional Simulation Code

Mayank Malik, Carlos Torres-Verdín, and Kamy Sepehrmoori, The University of Texas at Austin

Copyright 2006, Society of Petroleum Engineers

This paper was prepared for presentation at the 2006 SPE Annual Technical Conference and Exhibition held in San Antonio, Texas, U.S.A., 24–27 September 2006.

This paper was selected for presentation by an SPE Program Committee following review of information contained in an abstract submitted by the author(s). Contents of the paper, as presented, have not been reviewed by the Society of Petroleum Engineers and are subject to correction by the author(s). The material, as presented, does not necessarily reflect any position of the Society of Petroleum Engineers, its officers, or members. Papers presented at SPE meetings are subject to publication review by Editorial Committees of the Society of Petroleum Engineers. Electronic reproduction, distribution, or storage of any part of this paper for commercial purposes without the written consent of the Society of Petroleum Engineers is prohibited. Permission to reproduce in print is restricted to an abstract of not more than 300 words; illustrations may not be copied. The abstract must contain conspicuous acknowledgment of where and by whom the paper was presented. Write Librarian, SPE, P.O. Box 833836, Richardson, TX 75083-3836, U.S.A., fax 01-972-952-9435.

Abstract

This paper describes the development, testing, and successful application of a new compositional code for the numerical simulation of oil-base mud invasion and formation tester measurements that involve arbitrary miscibility between oil-base mud and native oil. The simulator assumes axial-symmetric variations of petrophysical properties as well as axial-symmetric flow-rate sources and boundary conditions. However, there are no restricting assumptions to the degree of miscibility between the fluids involved in the simulations. We solve the time-space evolution of component concentration with a time-marching implicit pressure explicit concentration (IMPEC) scheme. This method of solution considers the complete equations of state and implements rigorous and efficient flash calculations to describe the thermo-dynamical evolution of the various compositional phases due to space-time variations of pressure and concentration.

Simulations described in this paper consider the process of oil-base mud-filtrate invasion into reservoirs containing mixtures of connate water and oil. Subsequently, we simulate formation tester measurements by enforcing fluid withdrawal through the dual-packer section of the tester. Measurements consist of fluid pressure, fractional flow rates, fluid density, and fluid viscosity. Examples of application include homogenous and multi-layer formations as well as a capillary-transition zone. Comparison of simulation results against those obtained with a commercial code confirms the efficiency, accuracy, and reliability of our simulator.

Sensitivity analysis indicate that time evolution of fractional flow rates, fluid density, and fluid viscosity measured with the formation tester remain influenced by the petrophysical properties of the formation as well as by relative permeability and capillary pressure. The simulations described in this paper

accurately predict the measurement times necessary for the acquisition of clean samples of native formation oil in the presence of invasion and heterogeneous spatial distributions of petrophysical and rock-fluid properties.

Introduction

Formation testers are widely used to measure pressure, estimate reservoir permeability and permeability anisotropy, and to detect spatial variation of hydraulic connectivity through pressure transient testing.^{1,2,3,4,5,6} Often, formation-tester measurements remain influenced by the process of mud-filtrate invasion that takes place prior to measurement acquisition. Mud-filtrate invasion occurs in reservoirs penetrated by a well that is hydraulically overbalanced by mud circulation. In the case of water-base muds (WBM), the invading mud is immiscible with respect to the formation hydrocarbons and hence provides isolation from native hydrocarbons. However, in the case of oil-base muds (OBMs), the invading mud is miscible with the formation oil and does not provide proper isolation from native hydrocarbons. In addition, OBMs and synthetic-base muds (SBMs) induce changes in fluid viscosity and fluid density that can lead to erroneous estimates of permeability. OBMs and SBMs are increasingly being used in deep drilling operations around the world, including the Gulf of Mexico,⁷ due to faster penetration, inhibition of shale chemical alteration, and good wellbore stability.⁶ Thus, it becomes imperative to accurately model their effect on the invasion process and, subsequently, on formation tester measurements such as fluid sampling.

Previous work on formation testing has predominantly focused on simulating immiscible flow.^{8,9,10,11,12} Due to the complexity of miscible flow¹³, limited work has been advanced to simulate invasion by OBMs. Chin et al.¹⁴ introduced a strategy to quantify clean fluid sampling times in the presence of miscible flow. However, their algorithm was based on the assumption of only one hydrocarbon component and did not take into account changes in density or viscosity due to changes in pressure. Wu et al.⁴ modeled single component OBMs using an immiscible mud-filtrate invasion model and a commercial compositional code to simulate formation tester measurements and to estimate permeability, relative permeability, and capillary pressure. Proett et al.¹⁵ quantified optimal clean fluid sampling times in the presence of OBM invasion based on the component concentration of a single-component OBM.

The work presented in this paper is, to the best of our knowledge, the first study that simulates multi-component OBMs encompassing component PVT properties and mud-filtrate invasion together with changes in fluid density and fluid viscosity due to changes of hydrocarbon concentration and pressure. The simulations assume axial-symmetric variations of both petrophysical properties and flow-rate sources. These assumptions are not restrictive to quantify fundamental properties of formation-tester measurements including the time evolution of fluid sampling at the sand face. We consider five different hydrocarbon components in the formation and use field data to assign specific PVT properties of OBM invading the formation. Hydrocarbon phase compositions are tracked using the Peng-Robinson¹⁶ equation of state (EOS) wherein a mixing rule takes into account changes of fluid viscosity. Phase density is calculated from the EOS to account for variations of fluid density due to pressure changes.

In the sections to follow, we describe the simulation methodology and introduce a base case of formation properties to quantify the accuracy, reliability, and performance of our simulation code. Subsequently, we consider cases of multi-layer and capillary transition zones to assess the impact of formation petrophysical properties on the time evolution of fluid properties due to fluid pumpout with a dual-packer formation tester.

Methodology

We make use of an IMPEC technique to solve for the primitive unknowns, namely oil pressure and component compositions. After the overall composition of each component is obtained, we perform a phase equilibrium calculation to determine the phase composition of each component and the corresponding phase saturation. A rigorous Gibbs stability test is performed using reduced parameters¹⁷. Subsequently, we carry out all flash calculations in order to determine the number of phases. The formulation and the algorithm used in this simulator are similar to those of UTCOMP¹⁸, however, our algorithmic formulation is specifically designed to approach the case of null azimuthal variations of formation properties with respect to the axis of a vertical borehole. In addition, our formulation enforces boundary and source flow-rate conditions on specific depth segments along the wellbore. The outer limits of the reservoir consist of impermeable zones with no-flow boundary conditions.

In the formulation, we assume n_c hydrocarbon components and n_p phases excluding aqueous phase, with negligible mass fluxes (dispersion and mutual solubility) between water and other phases. Moreover, given that, in general, heat capacity of formation rocks is much larger than that of fluids present, we assume that space-time variations of temperature are negligible. Finally, we assume that there are no chemical reactions between the OBM and the native formation oil.

Darcy's law for multiphase flow in porous media governs the time-space evolution of pressure and concentration. Based

on the above-described assumptions, the partial differential equation for pressure is given by

$$\left(V_p c_f - \frac{\partial V_t}{\partial P} \right) \frac{\partial P}{\partial t} + V_b \sum_{i=1}^{n_c+1} \bar{V}_i \bar{\nabla} \cdot \sum_{j=1}^{n_p} (\xi_j x_{ij} \bar{u}_j) - \sum_{i=1}^{n_c+1} \bar{V}_i q_i = 0, \quad \dots (1)$$

where:

V_p is the pore volume,

c_f is the formation compressibility,

$\frac{\partial V_t}{\partial P}$ is the partial derivative of total fluid volume with

respect to pressure,

P is fluid pressure,

t is time,

V_b is bulk volume,

ξ_j is the molar density of phase j ,

x_{ij} is the mole fraction of component i in phase j ,

\bar{u}_j is the macroscopic Darcy velocity of fluid phase j ,

\bar{V}_i is the partial derivative of total fluid volume with

respect to component i , and

q_i is the molar flow rate of component i .

In addition, the mass conservation equation for the net change of component i is expressed in moles as

$$\frac{\partial N_i}{\partial t} + V_b \sum_{j=1}^{n_p} \bar{\nabla} \cdot (\xi_j x_{ij} \bar{u}_j) - q_i = 0 \text{ for } i=1, \dots, n_c+1 \quad \dots (2)$$

where N_i is the number of moles of component i per unit pore volume and is given by

$$N_i = \sum_{j=1}^{n_p} (S_j x_{ij} \xi_j), \quad \dots (3)$$

where S_j is the saturation of phase j .

In the above equations, molar density is calculated from the compressibility factor (Z_j) obtained from the Peng-Robinson-EOS, namely,

$$\xi_j = \frac{P}{Z_j R T}, \quad \dots (4)$$

where R is the universal gas constant and T is the reservoir temperature. On the other hand, mass density is computed from the molar density as

$$\rho_j = \xi_j \sum_{i=1}^{n_c} x_{ij} M_i, \quad \dots (5)$$

where M_i is the molecular weight of the hydrocarbon component. Thus, hydrocarbon mass density depends on the component concentrations as well as on reservoir pressure.

We calculate oil viscosity of component j , μ_j , assuming a quarter-power mixing rule¹⁹ applied to the sum of concentration of component i in each phase, i.e.

$$\mu_j = \left[\sum_{i=1}^{n_c} x_{ij} \cdot \mu_i^4 \right]^{1/4}. \quad \dots (6)$$

The component viscosities μ_i are calibrated to specific values of reservoir temperature and pressure using the Lohrenz-Bray-Clark²⁰ (LBC) correlation. Finally, we enforce mass conservation with the volume constraint

$$\sum_{j=1}^3 \left\{ \frac{N_j}{\xi_j} \right\} = 1.0 \quad \text{for } j = 1, 2, 3 \quad \dots(7)$$

where the subscript j designates water, oil, and gas phases, respectively.

We make use of a finite-difference discretization in cylindrical coordinates to solve numerically the pressure and concentration equations (Eqs. 1 and 2). The formulation neglects azimuthal variations of pressure, concentration, or petrophysical properties, and makes use of one-point upstream discretization in space and time. We solve the ensuing implicit pressure equation with a bi-conjugate stabilized²¹ matrix solver. Convergence of the matrix solver is diagnosed with the relative magnitude of the residual vector. According to this formulation, we solve Eqs. 4-7 at each node of the finite-difference discretization grid and at every time step with concomitant updates of fluid properties based on flash calculations.

Numerical Simulation of Mud-Filtrate Invasion and Fluid Pumpout

We simulate the process of OBM-filtrate invasion with flow rates of invasion calculated on the basis of specific formation and mud properties. The process of invasion gives rise to an initial spatial distribution of phase concentrations and pressure in the invaded formation. Subsequently, these spatial distributions are used as initial condition to simulate formation-tester measurements. Figure 1 shows the finite-difference grid (vertical and radial directions) used in the simulations for the case of a homogeneous and isotropic rock formation together with the location of the formation tester in a vertical well. The wellbore radius is equal to 0.35 ft. For the numerical simulations, we make use of a finite-difference grid consisting of 50 nodes in the radial direction and 45 nodes in the vertical direction. In keeping with the rapid space-time variations of pressure and concentration in the near-borehole region, radial nodes are logarithmically spaced from the wellbore to the outer grid boundary (located 1000 ft away from the axis of the borehole); along the vertical direction, grid nodes are spaced uniformly. As described in Fig. 2, the assumed dual-packer formation tester consists of one pressure-monitoring probe located 4 ft above the dual-packer module. The vertical opening of the dual packer is equal to 2.5 ft. Pressure and fluid sampling are simulated at the sandface of the center point of the dual-packer opening. A constant time step equal to $1e-4$ days is used to perform all the simulations described in this paper.

We consider a volume-averaged flow-rate of mud-filtrate invasion across the borehole wall prior to simulating formation-tester measurements. The calculation of the invasion flow rate is based on the flow initiation pressure method described by Roy and Sharma²² and Wu et al.⁴ with an overbalance mud pressure approximately equal to 3.8 psi for the Base Case.

As shown in Fig. 3, mud-filtrate invasion takes place during 36 hours with a flow rate of $5 \text{ ft}^3/\text{day}$, followed by fluid drawdown (pumpout) imposed with the dual-packer module

for 58 minutes with a flowrate of $75 \text{ ft}^3/\text{day}$. The drawdown is followed by a shut-in stage of 1.63 hours. We assume that the original formation hydrocarbons consist of components in the range from C_6 to C_{30+} . These hydrocarbons are lumped into five different components (C_{6-9} , C_{10-13} , C_{14-18} , C_{19-29} , and C_{30+}) using their pseudo properties summarized in Table 1. The binary-interaction parameter between the hydrocarbon components is assumed null. We make use of actual field data to assign component concentrations for the OBM that mixes with the assumed hydrocarbon formation components thereby changing the oil density and viscosity.

Specific numerical simulations considered in this paper include the following formation models:

1. Homogeneous and isotropic formation at irreducible water saturation (Base Case formation model).
2. Multi-layer formation at irreducible water saturation.
3. Homogeneous and isotropic formation at variable fluid saturation within a capillary transition zone.

Figures 4 and 5 show the assumed oil-water relative permeability and capillary pressure curves, respectively, for the simulations considered in this paper. In both cases, the assumed irreducible water saturation is 0.2. The OBM and the formation oil are first-contact miscible, whereupon no capillary pressure or relative permeability effects exist within the hydrocarbon phase.

Homogeneous formation at irreducible water saturation (Base Case)

Tables 1, 2, and 3 summarize the PVT, geometrical, and petrophysical parameters, respectively, assumed in the simulations of the Base Case formation model (isotropic and homogenous formation). The objective of this simple model example is to quantify the accuracy, reliability, and physical consistency of the simulations of OBM-filtrate invasion and dual-packer formation tester measurements.

Figure 6 displays the radial profile of C_{14-18} fraction with respect to radial distance in the formation at uniform time intervals of 0.96 hours during the invasion process. The dominant component in the OBM is C_{14-18} and is used to assess radial length of invasion in the formation. We observe that the radial length of invasion of that component is approximately 1.2 feet at 1.5 days after the onset of invasion. The radial length of invasion is a nonlinear function of the formation petrophysical properties. Figures 7, 8, and 9, compare the time evolutions of pressure, fluid density, and fluid viscosity, respectively, calculated with our simulator (identified as Near Wellbore Compositional Simulator, or NWCS, in the plots) against those calculated with the commercial simulator CMG-GEM[†]. Results indicate a good match between the two simulators. Figure 10 shows the time evolution of the concentration of various hydrocarbon components during fluid pumpout at the sandface of the dual-packer module. These simulations indicate gradual time variations of component concentration starting from those of the OBM filtrate and asymptoting toward the concentration of

[†] Copyright by Computer Modelling Group

native hydrocarbon components. Within approximately one hour of fluid pumpout all component concentrations have reached native component concentrations.

For the simulations considered in this paper, we define the time variations of sample quality as a function of the oil mass density via the expression

$$S(t) = \frac{\rho_{oi} - \rho_o(t)}{\rho_{oi} - \rho_{of}}, \quad \dots (8)$$

where:

$S(t)$ is the sample quality during fluid pumpout,

ρ_{oi} is the oil density at the end of invasion,

ρ_{of} is the native formation oil density, and

$\rho_o(t)$ is the oil density during fluid pumpout.

Initially, OBM is produced at the sandface during fluid pumpout and, as displayed in **Fig. 11**, the late-time behavior of sample quality asymptotes toward 100% concentration of clean formation components.

Sensitivity to permeability anisotropy ratio: We perform simulations to assess the sensitivity of pressure and sample quality to permeability anisotropy. This was done by decreasing the vertical permeability of the Base Case to 1 mD thereby yielding an anisotropy ratio (k_h/k_v) equal to 5. Remaining simulation parameters are the same as those of the Base Case formation model. **Figure 12** shows that the decrease of vertical permeability caused the pressure differential to increase. Likewise, as shown in **Fig. 13**, sample quality increases faster than in the Base Case formation model because of the corresponding decrease of vertical cross flow.

Multi-layer formation at irreducible water saturation

Figure 14 describes the multi-layer formation model consisting of three hydraulically communicated layers that exhibit the same values of porosity but different values of permeability. We assume that the water-oil capillary pressure and relative permeability curves are the same for the three layers (**Fig. 4**). **Table 4** summarizes the geometrical and petrophysical properties assumed for the three layers. In the simulations, the dual-packer opening is situated at the center of each layer in the vertical well. The purpose of this formation model is to quantify the influence of porosity and permeability on the time evolution of pressure, fluid density, and fluid viscosity during fluid pumpout.

Figure 15 displays the pressure measurements at the packer within the three layers. **Figure 16** shows the simulated sample quality as a function of fluid pumpout time at the sandface of the three layers. We remark that the oil mass density varies as a function of the hydrocarbon component concentrations (**Eq. 5**). As fluid pumpout time increases, sample quality increases and the oil mass density approaches that of formation oil density. Sample quality is relatively lower in the high-permeability layer due to deeper invasion.

We consider an additional variation of the multi-layer formation model in which the three layers exhibit the same

values of permeability but different values of porosity. The horizontal and vertical permeability for all layers is equal to 5 mD. **Table 5** summarizes the geometrical and petrophysical properties assumed for the three layers. The sample quality (**Fig. 17**) calculated from oil density is conditioned by the porosity of the layers. Sample quality increases with an increase of porosity due to relatively shallower invasion. In all cases, sample quality increases with time to reach over 95% at the end of fluid pumpout. These simulations indicate that the interplay between permeability, porosity, and sample quality is important to diagnose the sampling time necessary to acquire a sufficiently clean and representative sample of native formation oil. For the multi-layer cases considered in this section, it takes approximately one hour of fluid pumpout before the sampling quality reaches a value of 95%.

Homogeneous formation with variable fluid saturation in a capillary transition zone

In this case, we assume that the water-oil contact is located at a depth of 6525 feet such that the initial water saturation exhibits a capillary transition zone (**Fig. 18**). The formation is located in the depth range between 6500 ft to 6522.5 ft, with the water-oil contact located just below the formation. Remaining petrophysical properties are the same as those described in **Table 3**. The objective of this case example is to quantify the influence of mobile water in the time evolution of component concentration during fluid pumpout. Presence of non-irreducible water saturation causes the water-oil capillary pressure and relative permeability curves to exert a measurable control on the mobility of native oil during both OBM-filtrate invasion and fluid pumpout.

Figure 19 shows the simulated pressure variation during fluid pumpout. The center of the dual packer is simulated at the depth 6511.25 ft and the probe is simulated at the depth of 6507.25 ft. We note that the pressure differential is 567 psi at the packer in this case compared to the pressure differential of 87.3 psi for the Base Case even though the assumed values of porosity and permeability are the same in the two cases. The variation of pressure differential is due to the lower relative mobility of the oil phase within the capillary transition zone. Also, the influence of such a relatively large pressure differential is observed in the oil density measured at the sandface (**Fig. 20**). There is a measurable increase in oil density at the end of fluid pumpout due to the drastic increase of pressure at the sandface that equilibrates with the formation pressure.

Figure 21 displays the fractional flow of water during pumpout. At early times of fluid pumpout, OBM is produced and the fractional flow of water is relatively low. By contrast, at late times the fractional flow increases due to the presence of free water in the formation.

Sensitivity to relative permeability and capillary pressure: We analyzed the sensitivity of sample quality to relative permeability and capillary pressure curves by perturbing the relative permeability and capillary pressure curves assumed in the previous examples. The perturbed curves, shown in **Figs. 22** and **23**, have the same end-point for both the oil relative

permeability and the water capillary pressure; however, the perturbed curves entail an increase of oil mobility at the same value of formation water saturation. We modified the water end-point relative permeability to entail the same mobility in the capillary transition zone as in previous cases. To facilitate comparisons, we identify previous simulation results with the label “Case 5” whereas the simulations obtained with the perturbed set of relative permeability and capillary pressure curves are identified with the label “Case 6”. The fractional flow of water at the packer (**Fig. 24**) decreases in Case 6 due to the higher capillary pressure of water and due to the increased mobility of the oil phase. **Figure 25** displays the sample quality for Case 5 and Case 6. Simulation results indicate that the time evolution of sample quality is significantly affected by the perturbations of capillary pressure and relative permeability. In addition, we observe that the time evolution of fractional flow of water is more sensitive to variations of mobility and capillary pressure than the time evolution of sample quality.

Summary and Conclusions

The following summary and concluding remarks stem from the developments and simulation examples considered in this paper:

1. We presented the first documented simulations of OBM invasion and fluid pumpout in oil-bearing formations that make use of a rigorous axial-symmetric compositional formulation with multi-component oils. Benchmarking exercises with a commercial simulator confirmed the accuracy and reliability of our predictions of dynamic behavior of pressure and fluid density during mud-filtrate invasion and fluid pumpout.
2. Simulation results indicate that time required to retrieve clean fluid samples of formation oil is governed by the petrophysical and properties of the tested formation as well as by the flow rates imposed during fluid pumpout. In addition, the dynamic behavior of fractional flow of water is largely conditioned by relative permeability and capillary pressure in reservoirs that are not at irreducible water saturation.
3. The assumptions of immiscible flow and time-constant fluid properties (e.g. density and viscosity) often used in commercial applications of formation testing can lead to biased estimates of absolute permeability in the presence of OBM invasion. Proper assessment of petrophysical properties requires quantitative understanding of the interplay of oil density, oil viscosity, component concentrations, phase mobility, and fractional flow of water on pressure transients measured during fluid pumpout.
4. The new simulator described in this paper can be used to plan the acquisition of formation-tester measurements, to assess the sensitivity of clean-fluid sampling times to petrophysical and rock-fluid properties in the presence of OBM-filtrate invasion, and to quantify variations of fluid density and viscosity due to variations of pressure during fluid pumpout.

Nomenclature

c_f	:	Formation Compressibility [1/psi]
K	:	Absolute permeability, [mD]
k_h	:	Horizontal permeability, [mD]
k_v	:	Vertical permeability, [mD]
k_h/k_v	:	Permeability anisotropy ratio, []
M_i	:	Molecular Weight of component i , [lbs/lb-mole]
n_c	:	Number of components, []
N_i	:	Number of moles of component i
n_p	:	Number of phases, []
P	:	Oil phase pressure, [psi]
P_c	:	Capillary pressure, [psi]
Q	:	Fluid flow rate [ft ³ /day]
q_i	:	Component molar injection rate [lb-moles/day]
R	:	Gas constant, [psi-ft ³ /lb-mole ^o F]
S	:	Phase saturation, [fraction]
S_o	:	Oil phase saturation, []
S_{or}	:	Residual oil saturation, []
S_w	:	Water Saturation, []
T	:	Temperature, [°F]
u_j	:	Darcy velocity of phase j
V_b	:	Bulk Volume, [ft ³]
V_p	:	Pore Volume, [ft ³]
V_t	:	Total Fluid Volume [ft ³]
\bar{V}_{ti}	:	Partial derivative of total fluid volume with respect to component i , [ft ³ /lb-moles]
x_{ij}	:	Mole fraction of component i in phase j , [fraction]
Z_j	:	Compressibility factor of phase j , []

Greek Symbols

τ_h	:	Hydraulic overbalance stress, [psi]
ϕ	:	effective porosity, [fraction]
μ_i	:	Viscosity of component i , [cp]
μ_j	:	Viscosity of phase j , [cp]
ρ_j	:	Density of phase j , [lb/ft ³]
ρ_{oi}	:	Oil density at the end of invasion, [lb/ft ³]
ρ_{of}	:	Formation oil density, [lb/ft ³]
ξ	:	Molar Density [moles/ft ³]
Φ	:	Potential [psi]

Acronyms

<i>CMG</i>	:	Computer Modelling Group
<i>EOS</i>	:	Equation of State
<i>GEM</i>	:	Generalized Equation-of-State Model
	:	Compositional Reservoir Simulator
<i>OBM</i>	:	Oil-based Mud
<i>NWCS</i>	:	Near Wellbore Compositional Simulator
<i>PVT</i>	:	Pressure, Volume, and Temperature
<i>SBM</i>	:	Synthetic-based Mud
<i>WBM</i>	:	Water-based Mud

Acknowledgements

We are thankful to Robert Brugman from CMG for his guidance with the CMG-GEM simulator. The work reported in this paper was funded by The University of Texas at Austin’s Research Consortium on Formation Evaluation, jointly sponsored by Aramco, Baker Atlas, BP, British Gas,

ConocoPhillips, Chevron, ENI E&P, ExxonMobil, Halliburton Energy Services, Marathon, Mexican Institute for Petroleum, Hydro, Occidental Petroleum Corporation, Petrobras, Schlumberger, Shell International E&P, Statoil, TOTAL, and Weatherford.

References

1. Ayan, C., Hafez, H., Hurst, S., Kuchuk, F., O'Callaghan, A., Peffer, J., Pop, J., and Zeybek, M.: "Characterizing Permeability with Formation Testers," *Oilfield Review*, Autumn 2001, p. 2-23.
2. Stewart, G. and Wittman, M.: "Interpretation of the Pressure Response of the Repeat Formation Tester," paper SPE 8362, presented at the 54th SPE Annual Fall Technical Conference and Exhibition, Las Vegas, Nevada, September 23-26, 1979.
3. Onur, M., Hegeman, P.S., and Kuchuk, F.J.: "Pressure-Transient Analysis of Dual Packer-Probe Wireline Formation Testers in Slanted Wells," paper SPE 90250, presented at the SPE Annual Technical Conference and Exhibition, Houston, Texas, September 26-29, 2004.
4. Wu, J., Torres-Verdin, C., Proett, M., Sepehrnouri, K., and Belanger, D.: "Inversion of Multi-Phase Petrophysical Properties Using Pumpout Sampling Data Acquired with a Wireline Formation Tester," paper SPE 77345, presented at the Annual Technical Conference and Exhibition, San Antonio, Texas, September 29-October 2, 2002.
5. Xian, C., Carniege, C., Al Raisi, M.R., Petricola, M., and Chen, J.: "An Integrated Efficient Approach To Perform IPTT Interpretation," paper SPE 88561, presented at the SPE Asia Pacific Oil and Gas Conference and Exhibition, Perth, Australia, October 18-20, 2004.
6. Sarkar, A. K., Lee, J., and Kasap, E.: "Adverse Effects of Poor Mudcake Quality: A Supercharging and Fluid Sampling Study," paper SPE 64227, SPE Reservoir Evaluation and Engineering, June 2000.
7. Cheung, P., Hayman, A., Laronga, R., Cook, G., Goetz, P., Marshall, M., Hansen, S., Lamb, M., Li, B., Larsen, M., Orgren, M., and Redden, J.: "A Clear Picture in Oil-Base Muds," *Oilfield Review*, 13, No. 4, 2-27, Winter 2001.
8. Gok, I.M., Onur, M., Hegeman, P.S., and Kuchuk, F.J.: "Effect of an invaded Zone on Pressure Transient Data from Multi-Probe and Packer-Probe Wireline Formation testers in Single and Multilayer Systems," paper SPE 84093, presented at the Annual Technical Conference and Exhibition, Denver, Colorado, October 5-8, 2003.
9. Goode, P.A., and Thambynayagam, R.K.: "Influence of an Invaded Zone on a Multiprobe Formation Tester," paper SPE 23030, presented at the SPE Asia-Pacific Conference, Perth, Australia, November 4-7, 1991.
10. Jackson, R.R., Banerjee, R., and Thambynayagam, R.K.M.: "An Integrated Approach to Interval Pressure Transient Test Analysis Using Analytical and Numerical Methods," paper SPE 81515, presented at the SPE 13th Middle East Oil Show & Conference, Bahrain, April 5-8, 2003.
11. Kuchuk, F.J., Ramakrishnan, T.S., and Dave, Y.: "Interpretation of Wireline Formation Tester Packer and Probe Pressures," paper SPE 28404, presented at the 1994 SPE Annual Technical Conference and Exhibition, New Orleans, Louisiana, September 25-26, 1994.
12. Proett, M.A., Chin, W.C., and Mandal B.: "Advanced Dual-Probe Formation Tester with Transient, Harmonic, and Pulsed Time-Delay Testing Methods Determines Permeability, Skin, and Anisotropy," paper SPE 64650, presented at the SPE International Oil and Gas Conference and Exhibition, Beijing, China, November 7-10, 2000.
13. Mullins, O.C., Schroer, J., and Beck, G.F.: "Real-Time Quantification of OBM Filtrate Contamination During Openhole Wireline Sampling by Optical Spectroscopy," presented at the 41st SPWLA Annual Logging Symposium, Dallas, Texas, June 4-7, 2000.
14. Chin, W. C., and Proett, M. A.: "Formation Tester Immiscible and Miscible Flow Modeling for Job Planning Applications," presented at the SPWLA 46th Annual Logging Symposium, New Orleans, Louisiana, June 26-29, 2005.
15. Proett, M.A., Chin, W.C., Wu, J., Manohar, M., and Belanger D.: "Sample Quality Prediction with Integrated Oil and Water-based Mud Invasion Modeling," paper SPE 77964, presented at the SPE Asia Pacific Oil and Gas Conference and Exhibition, Melbourne, Australia, October 8-10, 2002.
16. Peng, D. Y., and Robinson, J. D.: "A New-Constant Equation of State," *Industrial and Engineering Chemistry Fundamentals*, v. 15, no. 59, 1976.
17. Li, Y., and Johns, R. T.: "Rapid Flash Calculations for Compositional Modeling," paper SPE 95732, presented at the SPE Annual Technical Conference and Exhibition, Dallas, Texas, October 9-12, 2005.
18. Chang, Y. B., Pope, G. A., and Sepehrnouri, K.: "A Higher-Order Finite Difference Compositional Simulator," *Journal of Petroleum Science and Engineering*, v. 5, no. 1, 35-50, November 1990.
19. Todd, M. R., and Longstaff, W. J.: "The Development, Testing, and Application of a Numerical Simulator for Predicting Miscible Flood Performance," *Journal of Petroleum Technology*, v. 253, 874-882, July 1972.
20. Lohrenz, J., Bray, B. G., and Clark, C. R.: "Calculating Viscosity of Reservoir Fluids from their Compositions," *Journal of Petroleum Technology*, SPE 915-PA, 1171-1176, October 1964.
21. Van Der Vorst, H. A.: "Bi-CGStab: A Fast and Smoothly Converging Variant of Bi-CG for the Solution of Nonsymmetric Linear Systems", *SIAM Journal Scientific and Statistic Computing*, v. 13, no. 2, 631-644, 1992.
22. Roy, R. S., and Sharma, M. M.: "The Relative Importance of Solids and Filtrate Invasion on the Flow Initiation Pressure," paper SPE 68949, presented at the SPE European Formation Damage Conference, The Hague, Netherlands, 21-22 May, 2001.

Table 1: Summary of PVT properties of the hydrocarbon components assumed in this paper for the simulations of invasion and fluid pumpout.

	C ₆₋₉	C ₁₀₋₁₃	C ₁₄₋₁₈	C ₁₉₋₂₉	C ₃₀₊
Initial Concentration	0.5	0.32	0.08	0.05	0.05
Injecting Concentration	0.0068	0.0068	0.9167	0.0587	0.0107
T _c (K)	575	644	718	788	849
P _c (psi)	284.25	284.25	237.29	211.75	107.28
Acentric Factor	0.4141	0.5567	0.7259	0.8777	1.11
Molar Weight (lbs/lb-moles)	119	165.11	226.77	290.55	750
Component Viscosity (cp)	0.294	0.294	0.232	0.182	0.12
Binary Interaction Parameter	0	0	0	0	0

Table 2: Summary of geometrical and numerical simulation parameters assumed for the Base Case formation model described in Fig. 1.

Variable	Units	Value
Wellbore radius (r _w)	ft	0.35
External radius (r _e)	ft	1000
Reservoir thickness	ft	22.5
Datum depth	ft	6500
Water-oil contact	ft	7000
Number of nodes - radial axis	--	50
Number of nodes - vertical axis	--	45
Grid cell size - radial axis	ft	variable
Grid cell size - vertical axis	ft	0.5

Table 3: Summary of reservoir rock and rock-fluid properties assumed for the Base Case formation model described in Fig. 1.

Variable	Units	Value
Porosity	fraction	0.18
Radial permeability	mD	5
Vertical permeability	mD	5
Water density @ STP	lb/ft ³	64
Water compressibility	psi ⁻¹	3E-06
Initial water saturation	fraction	0.21
Water viscosity	cp	1.0
Formation compressibility	psi ⁻¹	1E-12
Production flow rate	ft ³ /day	75
Initial Reservoir Pressure	psi	3900
Reservoir Temperature	°F	160

Table 4: Summary of reservoir rock properties assumed for the multi-layer formation model with different values of permeability (Fig. 14).

Layer	Variable	Units	Value
Upper Layer	Radial permeability	mD	5
	Vertical permeability	mD	5
	Top location	ft	6500
	Bottom location	ft	6507.5
Middle Layer	Horizontal permeability	mD	20
	Vertical permeability	mD	5
	Top	ft	6507.5
	Bottom location	ft	6515
Lower Layer	Horizontal Permeability	mD	100
	Vertical Permeability	mD	5
	Top location	ft	6515
	Bottom location	ft	6522.5

Table 5: Summary of reservoir rock properties assumed for the multi-layer formation model with different values of porosity.

Layer	Variable	Units	Value
Upper Layer	Porosity	fraction	0.25
	Top location	ft	6500
	Bottom location	ft	6507.5
Middle Layer	Porosity	fraction	0.15
	Top location	ft	6507.5
	Bottom location	ft	6515
Lower Layer	Porosity	fraction	0.05
	Top location	ft	6515
	Bottom location	ft	6522.5

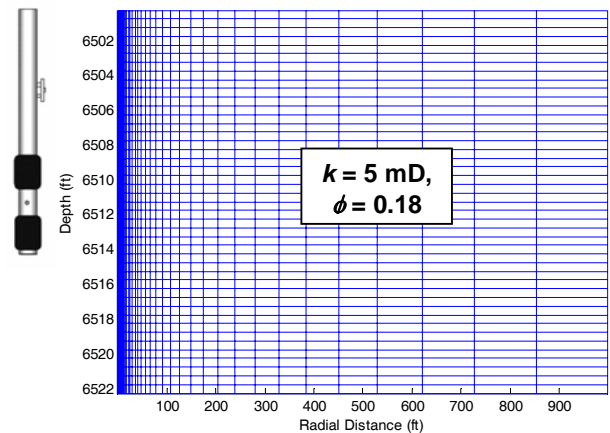


Figure 1: Description of the axial-symmetric finite-difference grid used in the simulations of OBM-filtrate invasion and dual-packer formation tester measurements. The values of absolute permeability (k) and porosity (φ) as well as the indicated depth range define the properties of the Base Case formation model considered in this paper.

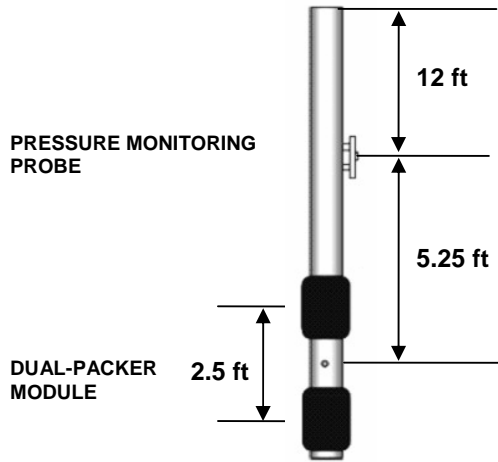


Figure 2: Configuration of the assumed dual-packer formation tester consisting of a vertical pressure monitoring probe and a dual-packer module. Pressure and fluid sensors are included in the dual-packer section of the formation tester.

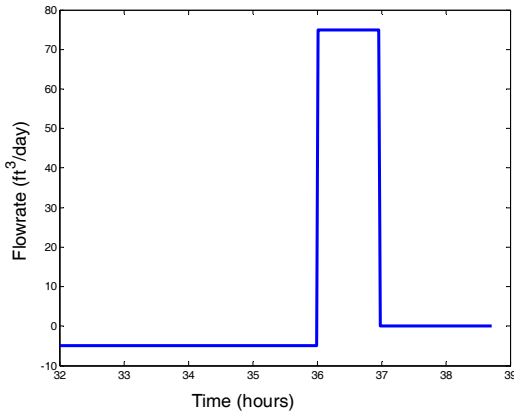


Figure 3: Flowrate assumed in the processes of mud-filtrate invasion and fluid pumpout (formation testing). Mud-filtrate invasion takes place during 36 hours followed by fluid pumpout for 58 minutes. The total simulation time is 38.6 hours.

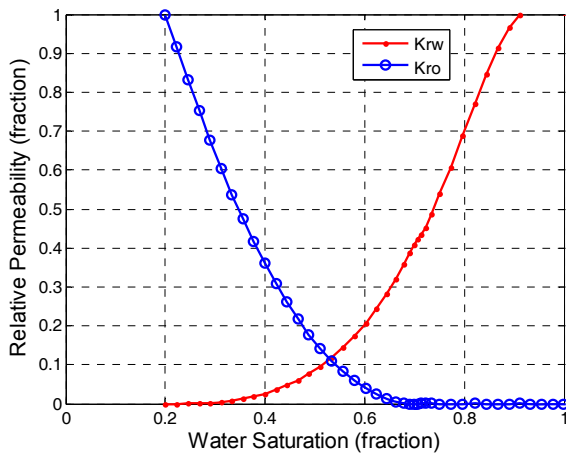


Figure 4: Water-oil relative permeability curves assumed in the simulations of mud-filtrate invasion and fluid pumpout.

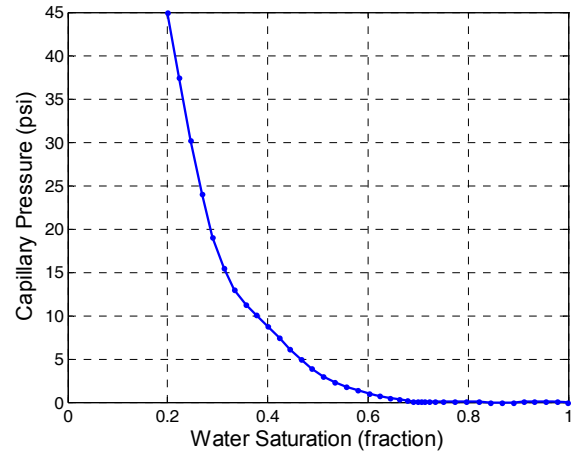


Figure 5: Water-oil capillary pressure curve assumed in the simulations of mud-filtrate invasion and fluid pumpout.

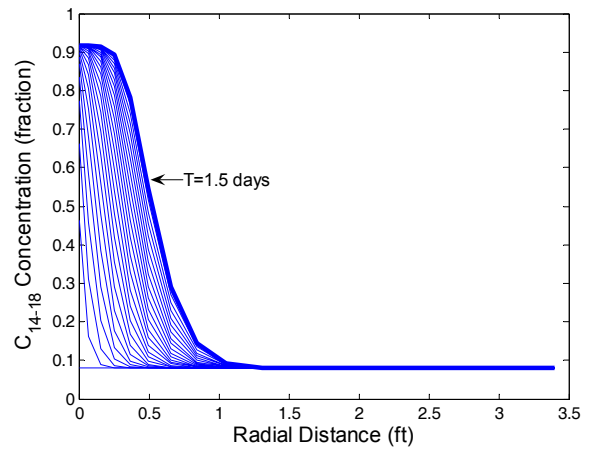


Figure 6: Variation of C_{14-18} component concentration during the process of mud-filtrate invasion for the Base Case formation model. The twenty-five curves shown in this figure correspond to radial profiles of the displayed OBM component at time increments of 0.96 hours after the onset of invasion.

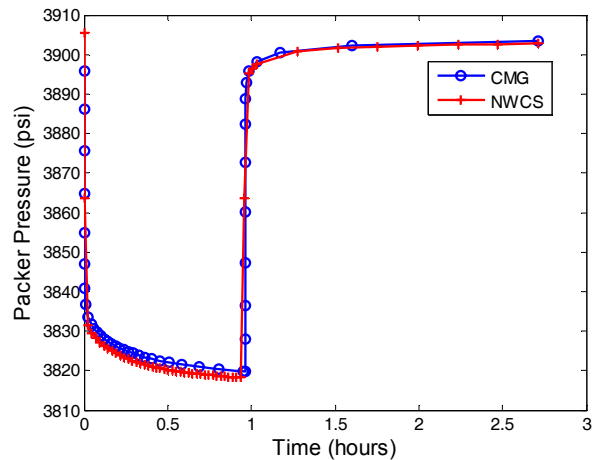


Figure 7: Comparison of pressure transient measurements at the packer calculated with CMG and the simulator developed in this paper (NWCS) for the Base Case formation model.

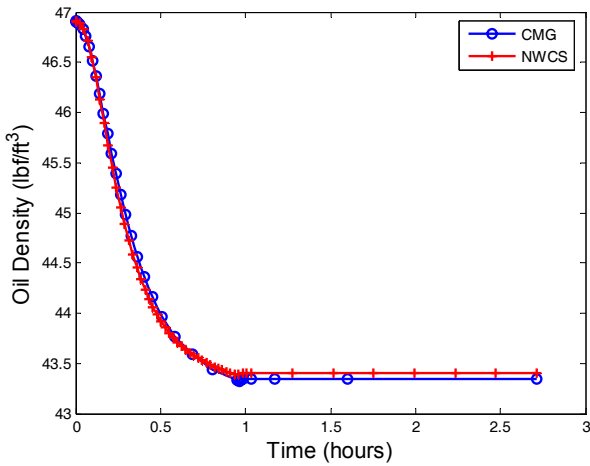


Figure 8: Comparison of the time evolution of oil density at the packer during fluid pumpout calculated with CMG and the simulator developed in this paper (NWCS) for the Base Case formation model.

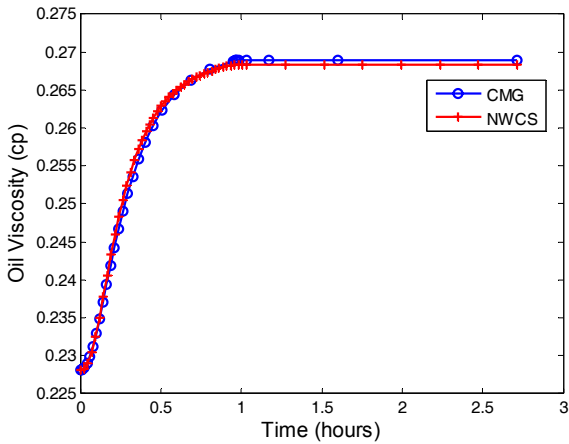


Figure 9: Comparison of the time evolution of oil viscosity at the packer during fluid pumpout calculated with CMG and the simulator developed in this paper (NWCS) for the Base Case formation model.

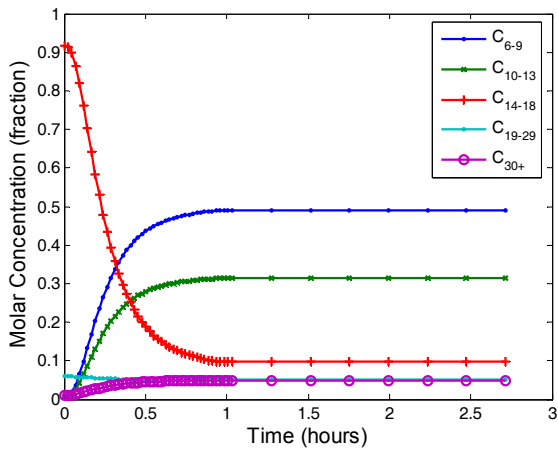


Figure 10: Time evolution of hydrocarbon component concentrations at the sandface during the process of OBM pumpout for the Base Case formation model. Concentrations vary gradually and reach the initial formation composition at the end of fluid pumpout.

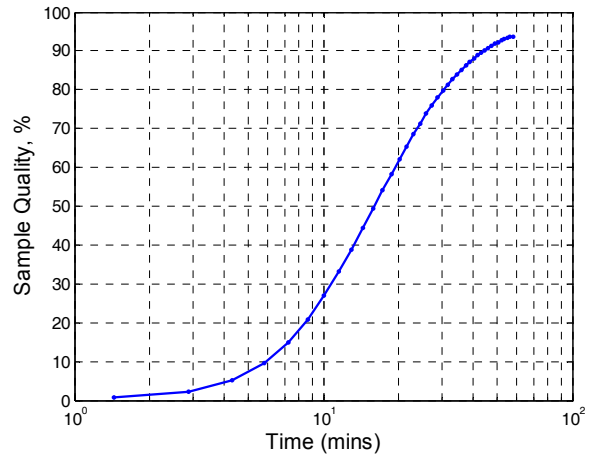


Figure 11: Time evolution of sample quality at the sandface during fluid pumpout for the Base Case formation model.

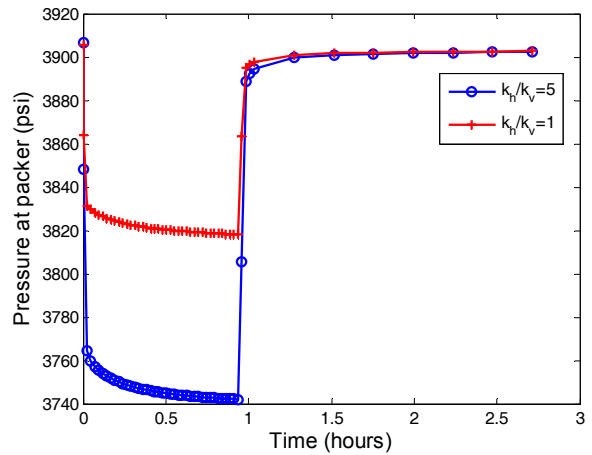


Figure 12: Sensitivity of packer pressure to permeability anisotropy (Base Case formation model). The vertical permeability is 1 mD for the case of anisotropic permeability.

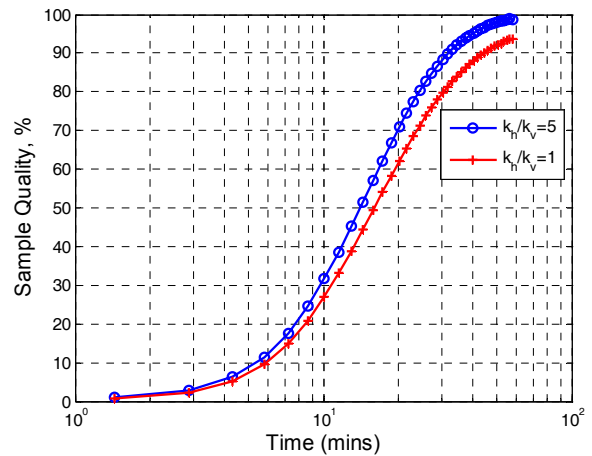


Figure 13: Sensitivity of the time evolution of sample quality to permeability anisotropy (Base Case formation model). The vertical permeability is 1 mD for the case of anisotropic permeability.

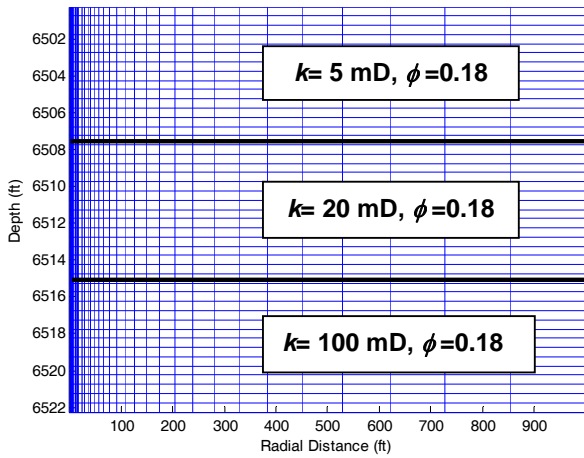


Figure 14: Three-layer reservoir model with different values of horizontal permeability (k = absolute permeability, and ϕ = porosity).

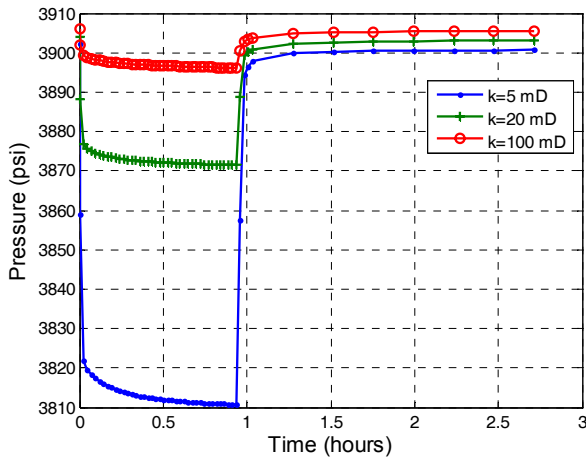


Figure 15: Simulated pressure transient measurements at packer locations centered within each of the three layers described in Fig. 14. The pressure differential varies due to layer permeability.

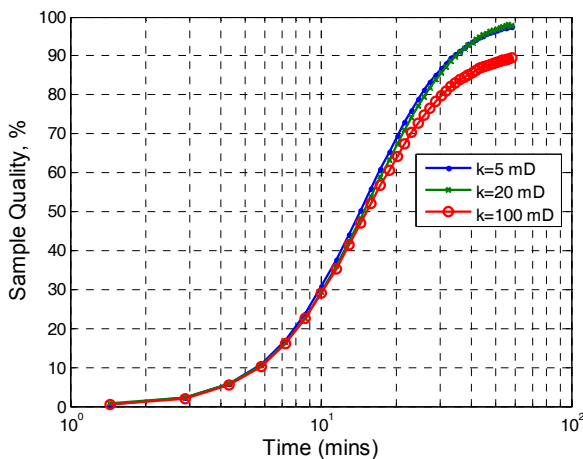


Figure 16: Time evolution of sample quality at the sandface during fluid pumpout as a function of layer permeability. The simulations were performed at packer locations centered within each of the three layers described in Fig. 14.

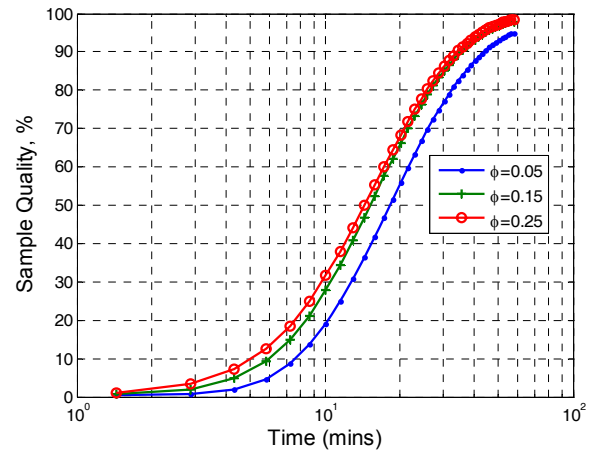


Figure 17: Sample quality at the sandface during fluid pumpout as a function of layer porosity. The simulations were performed at packer locations centered within each of the three layers described in Table 5.

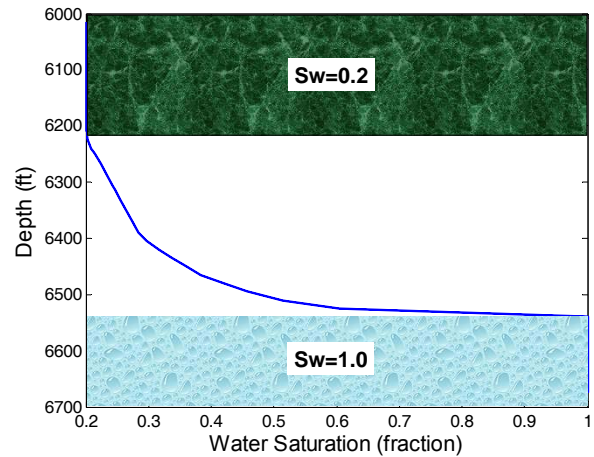


Figure 18: Variation of water saturation with respect to depth in a capillary transition zone. The formation varies from 6500 ft to 6522.5 ft and the water-oil contact is located at 6525 feet. The packer is deployed at the center of the formation (depth equal to 6511.25 ft).

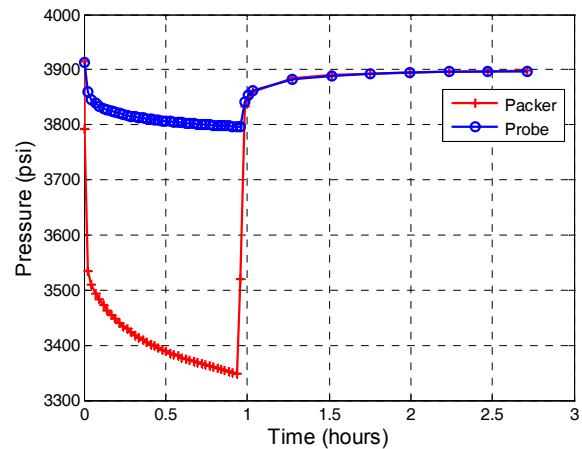


Figure 19: Pressure transient measurements simulated at the packer and monitoring probe within the capillary transition zone shown in Fig. 16.

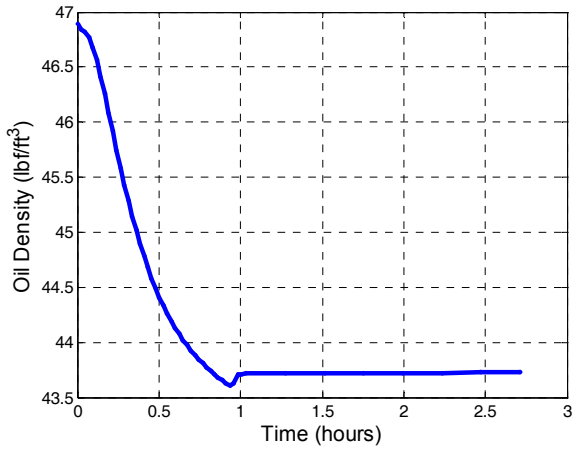


Figure 20: Time evolution of oil density as a function of time during fluid pumpout within the capillary transition zone described in Fig. 16. Note the increase in oil density at the end of fluid pumpout; this behavior is attributed to the rise in pressure at the wellbore that, in turn, increases the oil density at the sandface.

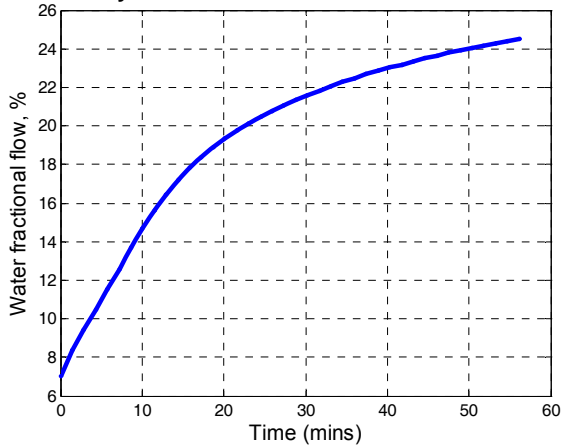


Figure 21: Time evolution of fractional flow of water at the sandface during fluid pumpout within the capillary transition zone described in Fig. 18. The fractional flow of water gradually increases until the end of fluid pumpout.

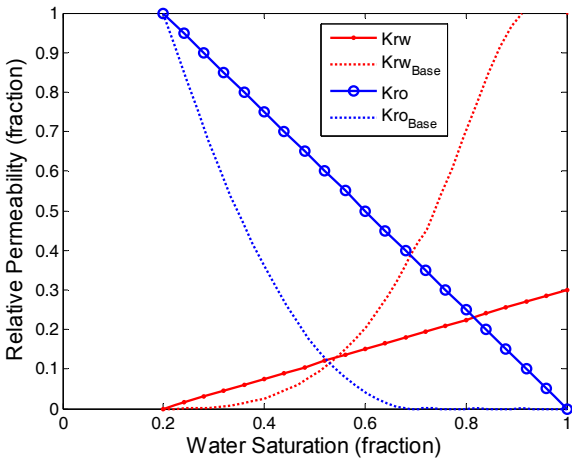


Figure 22: Water-oil relative permeability curves assumed in the sensitivity analysis of relative permeability compared to those of the Base Case.

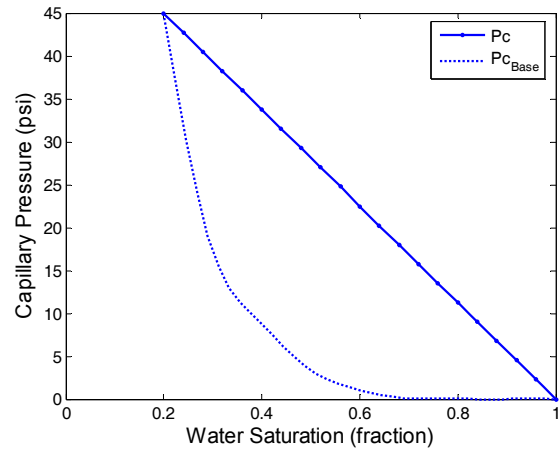


Figure 23: Water-oil capillary pressure curve assumed in the sensitivity analysis of capillary pressure compared to that of the Base Case.

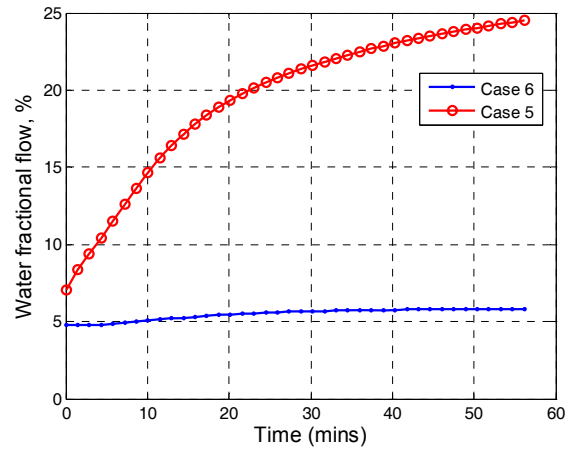


Figure 24: Time evolution of fractional flow of water at the sandface during fluid pumpout within the capillary transition zone described in Fig. 18. The curves describe fractional flow associated with perturbations of relative permeability (Fig. 22) and capillary pressure (Fig. 23) with respect to those of Case 5.

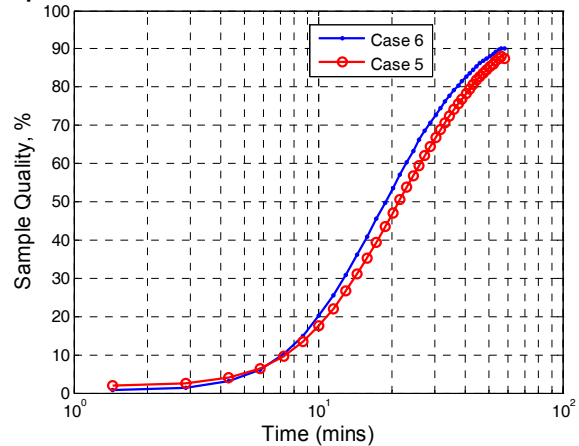


Figure 25: Time evolution of sample quality at the sandface during fluid pumpout within the capillary transition zone described in Fig. 18. The curves describe sample quality associated with perturbations of relative permeability (Fig. 22) and capillary pressure (Fig. 23) curves with respect to those of Case 5.